ELSEVIER

Contents lists available at ScienceDirect

Chemical Geology

journal homepage: www.elsevier.com/locate/chemgeo



Assessing the role of anoxia as a potential extinction driver in the shallow marine Neotethys during the Permian-Triassic mass extinction

Anja B. Frank ^{a,*}, Baran Karapunar ^b, Stephen E. Grasby ^c, Erdal Koşun ^d, Niko Lahajnar ^a, Mónica Alejandra Gómez Correa ^a, Stella Z. Buchwald ^a, Marc Metzke ^{a,e}, William J. Foster ^a

- ^a Universität Hamburg, Department of Earth System Sciences, Hamburg, Germany
- ^b School of Earth and Environment, University of Leeds, Leeds LS2 9JT, UK
- ² Geological Survey of Canada, Natural Resources Canada, Calgary, Alberta, Canada
- ^d Department of Geological Engineering, Akdeniz University, 07058 Antalya, Türkiye
- e Institute for Carbon Cycles, Helmholtz Centre Hereon, Geesthacht, Germany

ARTICLE INFO

Editor: Dr. Vasileios Mavromatis

Keywords:
Anoxia
Redox sensitive metals
REY
Permian-Triassic
Extinction
Neotethys
Türkiye

ABSTRACT

Anoxia has been hypothesised as a major kill mechanism for marine ecosystems during the Permian-Triassic mass extinction, but its importance is increasingly debated for shallow marine settings. For the Neotethys Ocean, in particular, geochemical data that is suitable to verify a local anoxic signal is lacking. Here, we investigated two shallow marine successions from the Antalya Nappes, Türkiye, for their redox sensitive metal and rare earth element and Yttrium (REY) composition to reconstruct local redox changes before, during and after the Permian-Triassic mass extinction. The investigated sections recorded reoccurring enrichments in the redox sensitive trace metals Re, U and Mo, supporting dynamic local redox conditions cycling between oxic and anoxic throughout the investigated Permian interval. No clear changes in redox conditions compared to the pre-extinction interval nor evidence of anoxic upwelling coinciding with the extinction event could be identified, questioning the role of anoxia as a local extinction driver. Above the extinction horizon, the sections were generally characterised by low redox sensitive metal enrichments and negative Ce anomalies revealing that post-extinction sediments were deposited in a consistently oxic environment. Hence, local anoxia within the shallow marine ecosystem of the Antalya Nappes appears not persistent enough around the extinction, and did not occur during the recovery. rendering it unlikely to explain biodiversity changes. Therefore, alternative environmental factor(s) should be considered as potential drivers of biodiversity changes for shallow marine ecosystems of the western Neotethys during the Permian-Triassic mass extinction and its recovery.

1. Introduction

The Permian-Triassic transition was marked by major climate perturbations, which have been linked to the eruption of the Siberian Traps Large Igneous Province, the related sill intrusion into carbon-rich sedimentary deposits (Burgess et al., 2017; Burgess and Bowring, 2015; Grasby et al., 2011; Svensen et al., 2023), and potentially also Palaeotethyan volcanism (Zhang et al., 2021). The volcanic activity led to the release of large volumes of greenhouse gases and volatile substances, which has been hypothesised to have caused significant environmental changes, such as increased temperatures (Gliwa et al., 2022; Joachimski et al., 2012), increased toxicity (Grasby et al., 2015) and expanded ocean anoxia (Wignall and Twitchett, 1996; Xiang et al., 2020) observed

in the rock record. These environmental changes, in turn, are commonly cited as potential drivers of the Permian-Triassic mass extinction, which was the most severe biodiversity crisis of the Phanerozoic, with major ecological changes, such as the decimation of reef ecosystems (Martindale et al., 2019), collapse of the latitudinal diversity gradient (Allen et al., 2023), poleward migration of Permian survival fauna (Foster et al., 2023), complete turnover in evolutionary faunas (Muscente et al., 2018), and major changes in the functional composition of marine ecosystems (Foster and Twitchett, 2014).

Widespread ocean anoxia, extending into shallow marine basins, has been widely accepted as a major driver of the extinctions within the marine realm since it was postulated in the 1990s and is still commonly cited to date (Isozaki, 1997; Knoll et al., 1996; Wignall and Hallam,

E-mail address: anja.frank@uni-hamburg.de (A.B. Frank).

^{*} Corresponding author.

1992; Wignall and Twitchett, 1996; Lau et al., 2016; Schobben et al., 2020; Xiang et al., 2020). Uranium (U) isotopes measured at multiple locations around the Palaeotethys (Brennecka et al., 2011; Lau et al., 2016; Zhang et al., 2020), Neothetys (Lau et al., 2016; Zhang et al., 2018b), and Panthalassa (Zhang et al., 2018a) support a modelled increase in the global extent of seafloor anoxia from 0.2 % to 20 % coinciding with the extinction (Lau et al., 2016). This supports that ocean anoxia could have played a key role in the observed loss of marine species. However, these results also indicate that oxygenated environments prevailed throughout the extinction. While U isotopes are an effective proxy to constrain global trends in seafloor anoxia, they are unsuitable to constrain the local redox conditions at a particular site, leaving the question whether and where anoxia developed in the shallow marine realm, where the fossil record and expression of the mass extinction is best recorded. Many local redox studies support the presence of anoxia or even euxinia in shallow marine basins (Algeo et al., 2007; Grice et al., 2005; Hays et al., 2007; Kump et al., 2005; Lau et al., 2016; Xiang et al., 2020; Grasby and Beauchamp, 2008), but an increasing number of studies have revealed locally oxic conditions during the extinction (Algeo et al., 2010; Heydari et al., 2003; Knies et al., 2013; Loope et al., 2013; Proemse et al., 2013; Yang et al., 2024). This questions the global role of anoxic conditions as an extinction driver in shallow marine ecosystems, revealing the need for site specific redox studies to properly understand its extent and, thus, role in shallow marine extinctions.

Most geochemical redox studies utilising local redox proxies on the Permian-Triassic transition are limited to the Palaeotethys, in particular to the South China Block (Chen et al., 2015; Li et al., 2016; Shen et al., 2007; Song et al., 2012; Xiang et al., 2020; Yang et al., 2024), resulting in a regionally-biased understanding of the role of anoxia as an extinction driver (Fig. 1). Redox interpretations for the shallow marine carbonate platforms of the Neothetys, on the other hand, have mainly been based on palaeontological data (Brosse et al., 2019; Gliwa et al., 2020; Krystyn et al., 2003; Richoz et al., 2010; Twitchett et al., 2004). While the presence of oxygen-sensitive benthic species is a good indicator that sufficient oxygen was present locally to support life, the loss of oxygensensitive species, infaunal bioturbation or changes in ecological traits do not necessarily indicate anoxia, or more accurately the loss of their aerobic habitat, as they could also be caused by other environmental or biotic stresses, such as increased sea surface temperatures or collapse of primary productivity (e.g., Foster et al., 2024; Hofmann et al., 2015a). Hence, interpretations of local redox changes based on palaeontological data across intervals of major environmental perturbations and biodiversity loss need to be tested using independent redox proxies.

Here, we study Permian-Triassic successions from Antalya, Türkiye, to reconstruct redox conditions in the shallow marine palaeo-equatorial setting of the Neotethys pre-, during and post- extinction. For this, we investigated enrichments in multiple redox sensitive metals (Re, V, U and Mo) as well as REY (rare earth elements and Yttrium) patterns (including Ce anomalies) at two shallow marine locations, Çürük Dağ and Öznurtepe (Fig. 1). The combination of multiple redox sensitive metals allows a test of different degrees of oxygenation as well as the differentiation between local anoxic development and upwelling of anoxic deep waters (Li et al., 2025; Tribovillard et al., 2012), while the addition of Ce anomaly data allows confirmation of locally oxic conditions, where applicable. Finally, the redox results were combined with available palaeontological data giving new insights into the potential connection between redox and biodiversity change.

2. Geological setting

The studied sites, Çürük Dağ and Öznurtepe, are part of the Antalya Nappe complex located in the Taurus Mountains in the province of Antalya, Türkiye (Fig. 1). The Antalya Nappes represent obducted oceanic and platform margin slope deposits of the former Neotethys (Şahin and Altiner, 2019; Stampfli et al., 1991), which was located at a

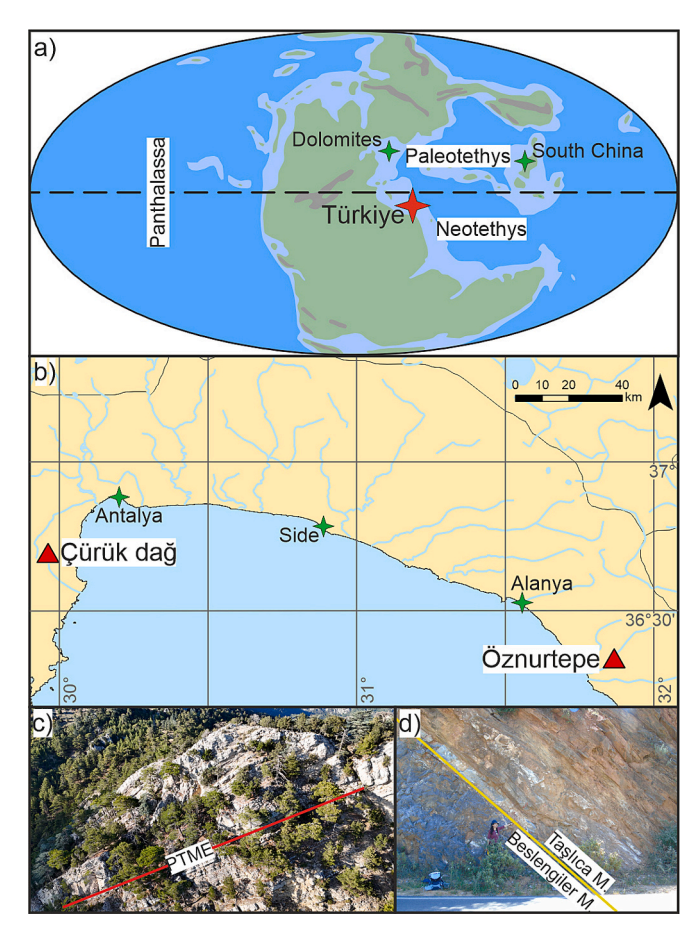


Fig. 1. a) Paleogeographic location of Türkiye during the Permian-Triassic transition (paleogeographic map from Blakey (2012)). b) Map of the study area with the locations of the investigated sections (WGS 1984). c) Aerial photograph of the Çürük Dağ cliff section with the Permian-Triassic mass extinction marked in red. d) Photograph of the Öznurtepe road section with the Beslengiler/Taşlıca member of the Sapadere Formation boundary marked in yellow. Person for scale. (For interpretation of the references to colour in this figure legend, the reader is referred to the web version of this article.)

near-equatorial latitude during the Permian-Triassic transition (Scotese and Langford, 1995). The sections studied at Çürük Dağ and Öznurtepe were deposited on the continental shelf in subtidal to supratidal environments, starting with platform carbonates in the Changhsingian, which are replaced by alternating oolite and microbialite beds at the Permian-Triassic transition (Karapunar et al., 2025). The sections record the Permian-Triassic transition as suggested by index fossils and the presence of a negative carbon isotope excursion that globally characterises the boundary (Crasquin-Soleau et al., 2002; Richoz, 2006).

Çürük Dağ is located in the Kemer district of Antalya, southwest of the city of Antalya (Fig. 1). Here, the Permian is represented by the Pamucak Formation (Figs. S1, 2), which constitutes a ~600 m thick middle-late Permian carbonate sedimentary succession (Lys and Marcoux, 1978) and is characterised by abundant fossils, including brachiopods, calcareous algae, bryozoans, foraminifera, gastropods, ostracods and echinoderms (Angiolini et al., 2007; Aubril and Angiolini, 2009; Crasquin-Soleau et al., 2004; Verna et al., 2011). The Changhsingian deposits of the Pamucak Formation are ~12 m thick (Richoz, 2006), based on the presence of the foraminifera Paradagmarita monodi, a low diversity brachiopod assemblage dominated by Spinomarginifera and Orthothetina, and the presence of Hindeodus cf. praeparvus (Angiolini et al., 2007). The Pamucak Formation primarily yields nodular limestone beds with variable amounts of fossil content, which alternate with thin mudstone layers (Karapunar et al., 2025). Between the

Changhsingian algal wackestones and packstones of the Pamucak Formation and the Changhsingian oolite, which marks the bottom of the Kokarkuyu Formation, an erosional surface was identified (Kershaw et al., 2011). The lowermost oolitic beds of the Kokarkuyu Formation are \sim 70 cm thick and include an impoverished Permian pre-extinction survival taxa (Angiolini et al., 2007). Furthermore, they are characterised by a negative $\delta^{13}C_{\text{carb}}$ excursion of 1–2% interpreted as the onset of the global carbon cycle disruption, which has commonly been correlated with the onset of the Permian-Triassic mass extinction event (Korte and Kozur, 2010; Richoz, 2006). The thin oolite interval at the bottom of the Kokarkuyu Formation is overlain by microbialite beds (Altiner and Zaninetti, 1981; Baud et al., 2005). These microbialite beds were dated to the earliest Triassic (Griesbachian) based on the presence of the conodonts *Hindeodus parvus*, *Isarcicella isarcica*, and *I. staeschei* (Crasquin-Soleau et al., 2002; Richoz, 2006).

The Öznurtepe sections are in the Gazipaşa district of Antalya (Fig. 1). The Permian deposits at this location are represented by the limestones of the Yüğlük Tepe Formation (Figs. S2, 3) (Özgül, 1985), which is dated as the latest Changhsingian based on the presence of *Paradagmarita monodi* (Groves et al., 2005). The Yüğlük Tepe Formation is overlain by the Sapadere Formation. Its lower parts are subdivided into the Beslengiler Limestone Member and the Taşlıca Member (Özgül, 1985). The base of the Beslengiler Member is marked by approximately 60 cm of Permian oolitic beds, which are followed by Triassic microbialites and oolite lithologies. The microbialites were dated as Early Triassic due to the presence of the foraminifera *Postcladella kalhori* (Groves et al., 2005). The Taşlıca Member is characterised by argillaceous limestones, varicoloured shales and limestones, yielding the molluscs *Unionites fassaensis*, *Claraia* sp., and *Ladinaticella costata* indicating Early Triassic age (Özgül, 1985).

Although the formation names differ between both sections, they are identical in terms of sedimentology and may be part of the same formations (Karapunar et al., 2025). Furthermore, this suggests that both sections recorded deposition under similar palaeogeographic and -environmental conditions. However, the sections in Öznurtepe is exposed to more tectonic deformation (Karapunar et al., 2025), possibly altering its original geochemical composition. A more detailed description of both sections, including field photos and thin section images can be found in Karapunar et al. (2025).

3. Material and methods

3.1. Analytical methods

At both localities two sections were sampled (Figs. S1, S2, Table 1). A total of 29 and 43 samples were taken for inorganic geochemical analysis at Çürük Dağ and Öznurtepe, respectively. The samples were generally between 2 and 5 cm thick and taken from undisturbed beds.

Bulk geochemical analyses were performed for all samples at the Geological Survey of Canada, Calgary. For this, any weathered surfaces were removed before the samples were crushed using a planetary ball mill with agate inserts. The powdered samples were digested in a 2:2:1:1 solution of $\rm H_2O\text{-}HF\text{-}HClO_4\text{-}HNO_3}$ and analysed for major minor and trace elemental compositions with a PerkinElmer Elan 9000 mass spectrometer (± 2 % precision). Total organic carbon (TOC) was determined using HAWK© (± 5 %) and Hg using a LECOR AMA254 mercury

Table 1Locations of the investigated sections at Çürük Dağ and Öznurtepe. The GPS coordinates denote the base points of the sampled sections.

Section	Latitude	Longitude	Altitude (m)
Çürük Dağ Cliff	N36°41.5374	E030°27.5563	1409
Çürük Dağ Crest	N36°41.5430	E030°27.6811	1429
Öznurtepe Road	N36°19.9719	E032°21.6019	126
Öznurtepe Creek	N36°19.8904	E032°21.4735	65

analyser (± 5 %).

Additionally, $\delta^{13}C_{carb}$ analyses were performed at the University of Hamburg on the samples from Öznurtepe as only limited $\delta^{13}C$ data exists for this locality (Demirtaş, 2018), all of which is Early Triassic and does not cover the extinction event (Fig. 3). For the $\delta^{13}C$ analysis, a sample piece was cut off and polished to create a fresh surface. Using a diamond-tipped drill, a micrite sample was taken. The carbon content of the samples was determined using a Euro EA 3000 (Euro Vector) elemental analyser (the precision for carbon is ± 0.05 %). For $\delta^{13}C_{carb}$ analysis, the samples were treated with suprapur 1 M HCl, combusted in an Elementar CHNOS Vario isotope elemental analyser at 950 °C, and analysed with an Elementar IsoPrime 100 isotope ratio mass spectrometer (the precision for $\delta^{13}C_{carb}$ is ± 0.05 %).

3.2. Proxy calculation

To evaluate potential diagenetic alterations through dolomitisation of the investigated carbonates, Mg/Ca ratios were calculated. Such ratios are commonly applied to assess the degree of dolomitisation, with dolostones commonly displaying Mg/Ca ratios close to or greater than 0.5 (e.g. Frank et al., 2021; Morse and Mackenzie, 1990; Rodler et al., 2017; Tostevin et al., 2016).

Enrichments in redox sensitive trace metals, such as U and Mo, can be used to track past redox fluctuations (e.g., Algeo and Li, 2020; Tribovillard et al., 2012; Tribovillard et al., 2006). However, when normalised to Al and a shale standard to calculate enrichment factors (EF), they commonly result in an artificially elevated EF within low-Al strata due to sediment dilution revealing a lithology bias (Krewer et al., 2024). As a result, revised enrichment factors (EF*) utilising excess rather than bulk redox sensitive metal (RSM) concentrations were recently proposed as an alternative method of calculating redox driven enrichments (Krewer et al., 2024). The EF* appear to mitigate the lithology bias in low-Al samples, while still resulting in similar values as traditional EF for high-Al samples (Li et al., 2025). Thus, EF* are increasingly applied to reconstruct palaeoredox (e.g. Buchwald et al., 2025; Frank et al., 2025) and were calculated here for Re, V, U and Mo using the elemental concentrations of the post Archean Australian shale (PAAS) as a standard (Taylor and McLennan, 1985) following the methods of Krewer et al. (2024):

$$RSM_{excess} = RSM_{sample} - (AI_{sample}^*(RSM_{PAAS}/AI_{PAAS}))$$
 (1)

$$\mathsf{EF_{RSM}}^* = (\mathsf{RSM}_{\mathsf{excess}} + \mathsf{RSM}_{\mathsf{PAAS}})/\mathsf{RSM}_{\mathsf{PAAS}} \tag{2}$$

Shale-normalised rare earth element and yttrium (REY) patterns can be used to identify whether marine sediments incorporated an authigenic seawater signal, as they have a distinct distribution in seawater (Elderfield and Greaves, 1982; Nothdurft et al., 2004; Tostevin et al., 2016). While typical seawater REY patterns display an increase from light to heavy rare earth elements, a depletion in Ce and an enrichment in Y, clays are characterised by flat normalised REY patterns (Tostevin et al., 2016). To calculate shale-normalised (SN) REY patterns for the investigated samples the REY concentrations of PAAS were used. Furthermore, Ce anomalies were calculated following the methods of Lawrence et al. (2006) as follows:

$$Ce/Ce^* = Ce_{SN}/(Pr_{SN}^*(Pr_{SN}/Nd_{SN}))$$
(3)

4. Results

4.1. Major elements

The Çürük Dağ sections are characterised by consistently high Ca (>37 wt%), but low Al content (<1 wt%), confirming the presence of calcitic carbonates with very little detrital input (Table S2, Fig. S3). Furthermore, the Mg/Ca ratio of all samples remained <0.2 and TOC <0.5 wt% throughout the investigated interval suggesting little

substitution of Ca by Mg through dolomitisation or organic matter accumulation, respectively. The Öznurtepe sections reveal a more variable geochemical composition (Table S2, Fig. S4). While the Yüğlük Tepe Formation and Beslengiler Member of the Sapadere Formation are generally characterised by Ca contents >30 wt%, the Taşlıca Member commonly records significantly lower Ca contents (as low as 10.6 wt%) above 40 m, reflecting the shift in lithology. Mg/Ca values up to 0.58 suggest diagenetic alteration between 42 and 45 m. The same interval also reveals a slight increase in Al up to 1.46 wt%, suggesting an increase in detrital input. Above 45 m, the Al content further increases up to 7.85 wt%, while Ca and Mg generally remain below 20 wt% and 0.8 wt%, respectively, reflecting a shift to a more siliciclastic lithology. TOC is consistently low (< 0.4 wt%) for all samples.

4.2. Carbon isotope record

The Öznurtepe sections recorded a wide range in $\delta^{13}C_{carb}$ between -7.19 and 3.39 % (Fig. 3, S4). The Yüğlük Tepe Formation is characterised by $\delta^{13}C_{carb}$ values around 3 % at the base of the investigated interval. At its very top, the formation records an abrupt ~1 % drop in $\delta^{13}C_{carb}$. Within the bottom of the Beslengiler Member of the Sapadere Formation, the $\delta^{13}C_{carb}$ values continue to gradually decrease. Above 21 m, the Beslengiler Member records a relatively stable $\delta^{13} C_{\text{carb}}$ trend around a value of ~ -0.5 ‰, except for the topmost sample, which is characterised by a $\delta^{13} C_{carb}$ values of -1.47 ‰. Previously reported δ¹³C_{carb} data for the Beslengiler Member confirm relatively stable $\delta^{13}C_{carb}$ for most of the member, except for the top ~50 cm, which are characterised by a recovery in $\delta^{13}C_{carb}$ up to 1.5 % (Demirtaş, 2018). The Taşlıca Member is characterised by highly variable $\delta^{13}C_{carb}$ values. The $\delta^{13}C_{carb}$ shifts repeatably, dropping to -7.19 % at 40.7 m only to recover to 1.34 % 10 cm above, before dropping back down to -6.13%, before eventually recovering to -1.14 % at the top of the investigated interval. Demirtas (2018) recorded an even wider range in $\delta^{13}C_{carb}$ values, however, considering the lithology change observed within the Taşlıca Member, the $\delta^{13}C_{carb}$ trend appears to be diluted by the isotopic signature of diagenetic carbonate cements rather than reflecting an

authigenic seawater signal.

4.3. Redox sensitive metal enrichments

At Cürük Dağ, the redox sensitive metal EF* of Mo and U reveal a decrease in metal enrichments between the Pamucak and Kokarkuyu formations (Fig. 2). The EF_{II}* of the Pamucak Formation range from 1.25 to 2.5, with most samples recording values >1.5, while the Kokarkuyu Formation samples are generally characterised by EF_{II}* <1.5, with only selected samples recording values up to 2.27. The EF_{Mo}* are also significantly lower for the Kokarkuyu Formation compared to the Pamucak Formation with maximal values up to 1.65 and 1.31, respectively, suggesting metal accumulation due to lower oxygen availability for the former. Furthermore, while most samples of the Pamucak Formation returned Mo concentrations above the detection limit (1 mg/kg), most Kokarkuyu Formation samples did not. Hence, large parts of the Kokarkuyu Formation did not incorporate detectable amounts of Mo, resulting in gaps in the record of EF_{Mo}*. A similar trend was observed for Re, with most Korkarkuyu Formation samples recording Re concentrations below the detection limit (0.001 mg/kg), while Re concentrations could be determined for most of the Pamucak Formation. The available EF_{Re}* data for both formations, however, reveal the same range of 3.5–11. The EF_V^* values of the investigated interval were consistently close to 1, providing no support for V accumulation due to deoxygenation.

The Öznurtepe sections reveal different trends in RSM EF* between the Yüğlük Tepe and Sapadere formations, but also between the Beslengiler and Taşlıca members of the Sapadere Formation (Fig. 3). The Yüğlük Tepe Formation is characterised by almost consistently enriched EF* for Re, U and Mo with values up to 23.5, 2.15 and 2.29, respectively. The EF $_{\rm V}^*$, on the other hand, generally plots close to 1, suggesting little sedimentary enrichment, with only selected samples recording elevated values up to 1.52. The Beslengiler Member of the Sapadere Formation generally displays ${\rm EF}_{\rm V}^*$ and ${\rm EF}_{\rm U}^*$ values close to 1, suggesting limited metal transfer to the sediment. This is further supported by the overall lack in ${\rm EF}_{\rm Re}^*$ and ${\rm EF}_{\rm Mo}^*$ data, due to Re and Mo concentrations being

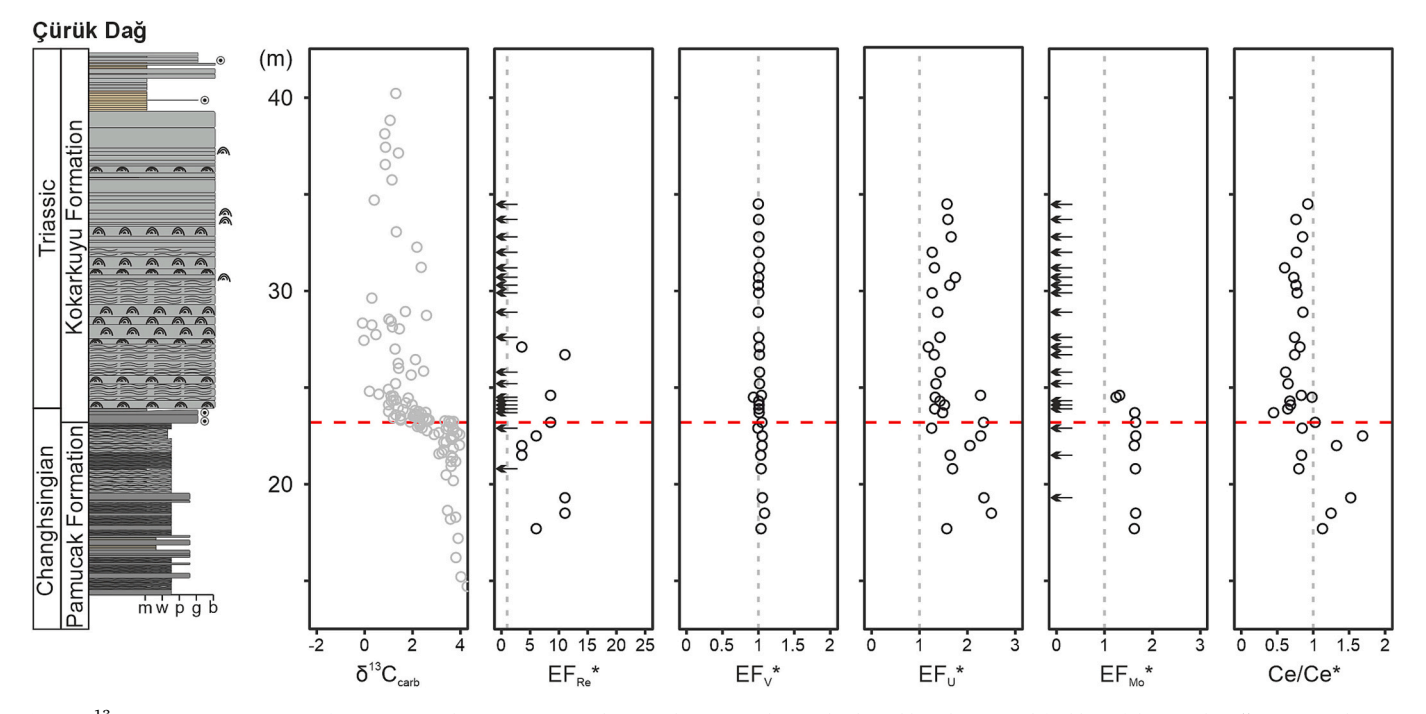


Fig. 2. 3^{13} C_{carb} (Demirtas, 2018; Richoz, 2006), redox sensitive metal EF* and Ce anomaly trends plotted besides a simplified log of the Çürük Dağ sections. The grey markers mark published data, the red dashed line the onset of the Permian-Triassic mass extinction and the grey dashed lines the threshold between enrichment/depletion compared to PAAS, while the arrows represent samples with RSM concentrations below the detection limit. (For interpretation of the references to colour in this figure legend, the reader is referred to the web version of this article.)

A.B. Frank et al. Chemical Geology 696 (2025) 123108

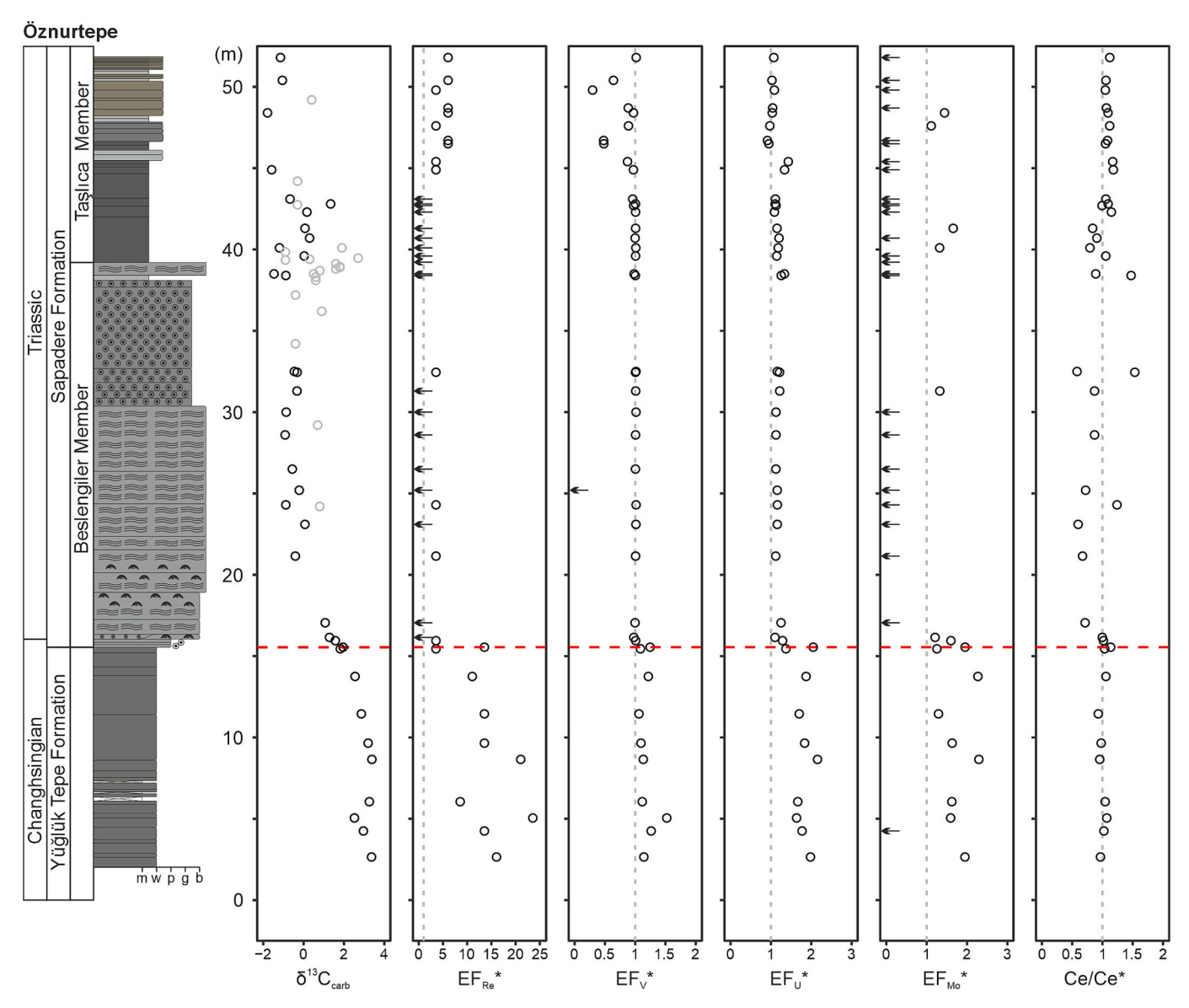


Fig. 3. $\delta^{13}C_{carb}$ (Demirtaş, 2018, this study), redox sensitive metal EF* and Ce anomaly trends plotted besides a simplified log of the Öznurtepe sections. The grey markers mark published data, the red dashed line the onset of the Permian-Triassic mass extinction and the grey dashed lines the threshold between enrichment/depletion compared to PAAS, while the arrows represent samples with RSM concentrations below the detection limit. The $\delta^{13}C_{carb}$ plot was scaled to focus on the $\delta^{13}C_{carb}$ data of the Yüğlük Tepe Formation and Beslengiler Member. For the full range in $\delta^{13}C_{carb}$ see Fig. S4. (For interpretation of the references to colour in this figure legend, the reader is referred to the web version of this article.)

below the detection limit. The bottom ${\sim}5$ m of the Taşlıca Member reveal similar RSM enrichment patterns as the Beslengiler Member, but its upper part is characterised by slightly different EF_{Re}^* and EF_V^* trends. In this interval Re is commonly above the detection limit revealing EF_{Re}^* up to 6, while the EF_V^* commonly records values ${<}1,$ suggesting a V depletion.

4.4. Rare earth elements and yttrium

The averaged REY patterns for the Pamucak and Kokarkuyu formations of Çürük Dağ reveal similar trends (Fig. 4). Both reveal overwhelmingly shale-like REY patterns (Nothdurft et al., 2004), however, the Kokarkuyu Formation also reveals a slight negative Ce anomaly as well as a modest increase from light to heavy rare earth elements, suggesting that remnants of an authigenic seawater signal were preserved (Nothdurft et al., 2004; Tostevin et al., 2016). The Pamucak Formation only recorded negative Ce anomalies indicative of oxic conditions in selected samples (Fig. 2). The Kokarkuyu Formation, on the other hand,

almost consistently recorded pronounced negative Ce anomalies. The Öznurtepe sections revealed significantly different averaged REY patterns for its Yüğlük Tepe and Sapadere formations. The Yüğlük Tepe Formation and Taşlıca Member of the Sapadere Formation are characterised by relatively flat shale-like REY patterns, suggesting that no authigenic seawater signal was preserved (Fig. 4). This is reflected in all the Yüğlük Tepe Formation samples and most Taşlıca Member samples recording Ce/Ce* values of ~ 1 (Fig. 3). The Beslengiler Member of the Sapadere Formation displays a more seawater-like REY pattern with a minor negative Ce anomaly and an overall increase from light to heavy REY. The Ce anomalies of the member record a wide range from 0.58 to 1.53, but most samples suggest a depletion in Ce with Ce/Ce* values generally < 0.9.

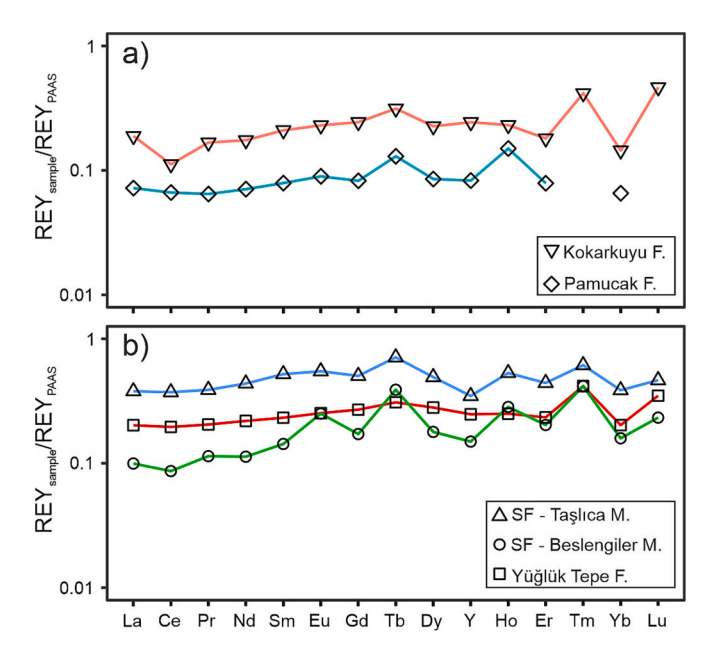


Fig. 4. PAAS-normalised REY patterns averaged for the Pamucak and Kokarkuyu formations at Çürük Dağ (a) as well as the Yüğlük Tepe Formation and Beslengiler and Taşlıca members of the Sapadere Formation at Öznurtepe (b).

5. Discussion

5.1. Proxy evaluation

One concern when utilising geochemical proxies to reconstruct past marine environmental conditions is, whether the chosen proxy captures an authigenic seawater signal, rather than a lithological or diagenetic one. Dolomitisation is commonly a problem when working with carbonate samples, but the generally low Mg/Ca ratios suggest little substitution of Ca in the investigated carbonates. Therefore, it is unsurprising that an ANOVA test revealed no significant correlation between Mg/Ca and the investigated redox proxies (df = 1, F < 3.61, p > 0.062), even when tested in dependence to section, formation or member. Hence, no evidence for a diagenetic alteration of the proxy signatures was observed.

Detrital overprinting can further mask an authigenic seawater signal. An initial one-way ANOVA test suggests a significant interaction of the detrital tracer Al and EF_V^* (df = 1, F = 111, p = $5*10^{-16}$) as well as EF_U^* (df = 1, F = 8.87, p = 0.004), suggesting that changes in these proxies are lithologically-controlled rather than redox-driven. For EF_V* the detrital tracer Al remains the most significant variable (df = 1, F > 108, $p < 2*10^{-15}$), even when considering other independent variables (site, formation or member) in a two-way ANOVA. However, considering that the calculation of EF* involves normalisation to Al to account for a detrital control, the suggested lithological control on EF_V* is likely not due to detrital overprinting directly, but rather due to deoxygenation in the study area being not pronounced enough to initiate a redox driven transfer of V into the sediment. Redox sensitive metal enrichments of modern marine sediments also support that V is generally less sensitive to reduced oxygen availability compared to e.g., U or Mo, commonly recording high EF_{V}^* only under euxinic conditions (Li et al., 2005). This would support that euxinia did not develop throughout the studied

In the case of EF_U*, the addition of other independent variables (site, formation or member) in a two-way ANOVA, reveal that the formation (df = 3, F = 32.84, $p = 4*10^{-13}$) or member (df = 4, F = 25.13, $p = 1*10^{-12}$) better explain variations in EF_U* than Al (df = 1, F < 2.55, p > 0.115). Hence, variation in the redox proxy appears to be controlled by factors such as pre- and post-extinction or passing time, rather than

lithology.

REY patterns, and thus Ce/Ce* values, are known to be very susceptible to detrital overprinting. However, no significant correlation was observed between Ce anomalies and Al (df = 1, F = 2.76, p = 0.101). On the other hand, most samples from Çürük Dağ and parts of Öznurtepe reveal flat shale-like patterns (Fig. 4). This could be in parts due to the use of bulk material rather than leachates of the authigenic fraction. Considering that the Pamucak and Kokarkuyu formations of Çürük Dağ, as well as the Beslengiler Member of the Sapadere Formation at Öznurtepe still reveal many samples with negative Ce anomalies within the range of Ce anomalies reported for marine carbonates globally (Wallace and Hood, 2017), the reported bulk Ce/Ce* appear to still be useful as a tracer for oxic seawater conditions in parts of the sections, despite its limitations.

5.2. Permian/Triassic boundary

Absolute age dating for the Permian-Triassic sedimentary succession of the investigated sites is lacking, rendering it challenging to determine the timing of the mass extinction relative to the Permian/Triassic boundary. Biostratigraphic constrains have been reported for Çürük Dağ, placing the deposition of the Pamucak Formation in the Permian (Angiolini et al., 2007). While the oolite beds at the base of the Kokarkuyu Formation still display remnants of a Permian fauna (Angiolini et al., 2007), the microbialites start to display Griesbachian biostratigraphic markers including Hindeodus parvus, Isarcicella isarcica, and I. staeschei (Crasquin-Soleau et al., 2002; Richoz, 2006), suggesting that the Permian/Triassic boundary is located somewhere between 0 and 70 cm above the formation boundary. Different marine organismal groups either completely disappeared in the studied sections (brachiopods, calcareous algae, bryozoans) or substantially decreased in diversity (molluscs, foraminifera, ostracods) with the onset of the oolite deposition (Angiolini et al., 2007; Crasquin-Soleau et al., 2004) at the Pamucak/Kokarkuyu formation boundary (Fig. S1), suggesting that the onset of the Permian-Triassic mass extinction event is marked by the formation boundary. Considering that the formation boundary displays evidence of an erosional surface (Kershaw et al., 2011), it is possible that part of the extinction event is not recorded at Çürük Dağ. However, the diversity drop from the Pamucak Formation to the Kokarkuyu Formation further coincided with a negative carbon isotope excursion (Demirtas, 2018; Richoz, 2006) (Fig. 2), which is commonly associated with the extinction event (Korte and Kozur, 2010). As the carbon isotope excursion does not show an abrupt drop, any time gap was comparatively short. The Kokarkuyu Formation at Çürük Dağ displays a significantly impoverished Permian fauna within its lowermost oolitic interval as well as no preservation of skeletal organisms in the stromatolites and thrombolites (Angiolini et al., 2007; Kershaw et al., 2012; Kershaw et al., 2011), clearly marking the formation as post-extinction.

Biostratigraphic constrains on the Öznurtepe sections are not yet available. However, the similar transition from algae-foraminifera dominated packstones in the Yüğlük Tepe Formation to oolites almost devoid of fossil followed by the appearance of microbialites in the Sapadere Formation at Öznurtepe (Fig. S2) supports that the Permian-Triassic mass extinction also coincides with the formation boundary. The $\delta^{13}C_{carb}$ data presented here, further reveal a negative excursion across the formation boundary, suggesting that, like Çürük Dağ, Öznurtepe recorded the carbon cycle perturbation typical for the late Permian concurrent to the extinction (Fig. 3).

5.3. Redox across the Permian-Triassic transition

The pre-extinction Pamucak and Yüğlük Tepe formations at Çürük Dağ and Öznurtepe generally reveal higher RSM EF* compared to the Kokarkuyu and Sapadere formations (Fig. 5), suggesting that the former were deposited under more reducing conditions. This is supported when conducting ANOVA tests, as these reveal that the redox proxies EF_{Re}^* ,

A.B. Frank et al. Chemical Geology 696 (2025) 123108

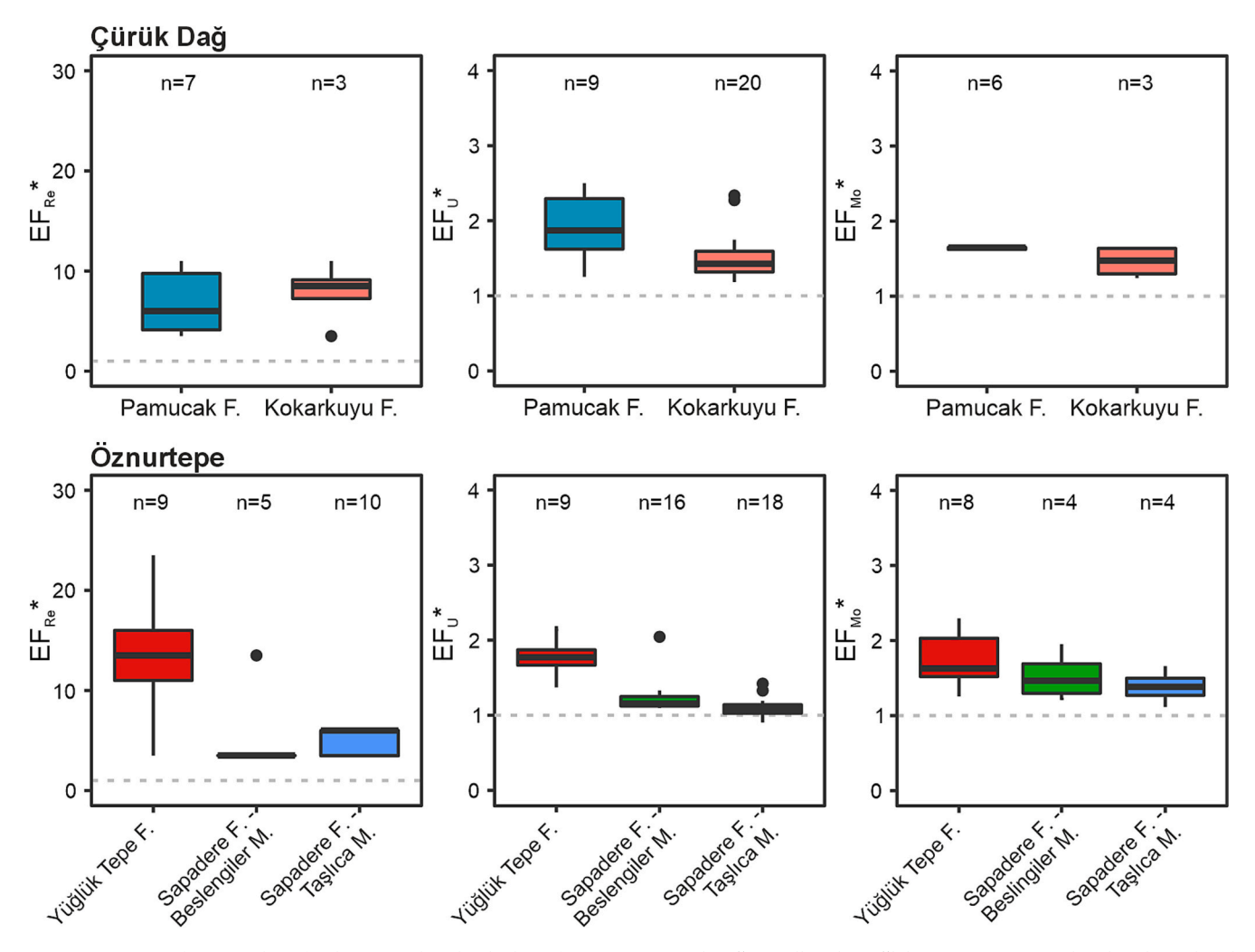


Fig. 5. Range in EF* of Re, U and Mo for the Pamucak and Kokarkuyu formations at Çürük Dağ as well as the Yüğlük Tepe Formation and Beslengiler and Taşlıca members of the Sapadere Formation at Öznurtepe.

 $\mathrm{EF_U}^*$ and $\mathrm{Ce/Ce}^*$ all show the highest dependence on formation (df ≥ 1 , F > 8.92, $p < 2^*$ 10^{-4}) at both sites rather than on site, member, dolomitisation (Mg/Ca) or lithology (Al). Considering that the formation boundary at both sites corresponds to the onset of the Permian-Triassic mass extinction, this indicates that there is a clear difference in redox conditions pre- and post-extinction. However, the suggestion of more reducing conditions pre-extinction appears contradictory considering that the pre-extinction interval is characterised by a rich fossil record, while the investigated post-extinction strata is almost void of fossils (Angiolini et al., 2007; Aubril and Angiolini, 2009; Crasquin-Soleau et al., 2004; Groves et al., 2005; Verna et al., 2011). Similar metal enrichment trends have also been observed for the Paleotethys, in the Dolomites (Frank et al., 2025), as well as South China (Xiang et al., 2020), demonstrating that elevated redox sensitive metal contents indicative of reduced oxygen can co-occur with a high fossil abundance.

As discussed above, the overall lack of $\mathrm{EF_V}^*$ indicates that redox conditions did not reach euxinic conditions, which is supported by comparatively low $\mathrm{EF_{Mo}}^*$ that are atypical for euxinia (Figs. 2, 3) (Tribovillard et al., 2012; Tribovillard et al., 2006). This excludes a development of photic zone euxinia as suggested at shallow marine localities in the Barents Sea and Tethys Ocean during the Permian-Triassic transition (Cao et al., 2009; Grice et al., 2005; Nabbefeld et al., 2010; Schobben et al., 2020). Alternatively, evidence for upwelling of oxygen depleted deep waters was reported for localities in Panthalassa and the Palaeotethys (Algeo et al., 2007; Knies et al., 2013). However, such a process is generally reflected in significant Mo enrichments over U (Li

et al., 2025; Tribovillard et al., 2012), but the EF* of Çürük Dağ and Öznurtepe consistently reveal similar or lower Mo enrichments over U enrichments. Therefore, the metal enrichments of Çürük Dağ and Öznurtepe support at best a local development of anoxia, free of euxinic conditions.

The decreasing trend in RSM EF* observed up section at Cürük Dağ and Öznurtepe, reveal a decrease in metal scavenging suggesting a shift to more oxic conditions. Throughout the late Permian, both locations are commonly characterised by elevated EF_U* and EF_{Mo}* compatible with EF* recorded for modern marine sediments deposited under highly dysoxic to anoxic conditions (Li et al., 2025), suggesting that anoxia prevailed leading up to and, potentially, during the Permian-Triassic extinction. At the same time, the EFRe* signatures of the Permian interval support at most dysoxic conditions and are even compatible with oxic conditions. Furthermore, at Çürük Dağ multiple samples recorded Re and Mo concentrations below the detection limit indicating that the redox conditions were not sufficiently reducing to result in a significant Re or Mo transfer to the sediment (Algeo and Li, 2020; Li et al., 2025). Multiple samples are also characterised by comparatively low EF_{II}* and negative Ce anomalies (Fig. 2, Table S1), supporting that oxic conditions occurred. Hence, the EF_U^* - EF_{Mo}^* pairings of the investigated Permian interval at Çürük Dağ support dynamic oxygen conditions cycling between oxic and anoxic conditions (Li et al., 2025). At Öznurtepe the RSM EF* revealed a similar pattern for the investigated Permian interval, except that negative Ce anomalies were not observed (Fig. 3). It is noteworthy, that at both sections the geochemical composition of the

lowermost sample above the extinction supports local anoxia at the bottom of the Kokarkuyu and Sapadere formations. On the other hand, the topmost samples of the Pamucak and Yüğlük Tepe formations reveal geochemical signatures suggesting the presence of oxic conditions right before the extinction. This poses the question whether the anoxic signal represents a development of anoxia that triggered the Permian-Triassic mass extinction or whether the return to more reducing conditions at the sediment interface was a consequence of the extinction itself? Resolving this, however, is complicated by the fact, that the lower surface of the post-extinction oolites at Çürük Dağ was identified as an erosional interface (Kershaw et al., 2011), suggesting that the section does not fully record the critical extinction interval.

The suggestion of dynamic redox conditions cycling between oxic and anoxic conditions in the late Permian of Çürük Dağ and Öznurtepe revealed by our samples contrasts with interpretations of continuous oxic conditions reported for the Demirtas sections (Loope et al., 2013). Demirtaş is located approximately 20 km north northwest of Öznurtepe, belongs to the same formations as Öznurtepe and has a similiar facies composition as Çürük Dağ and Öznurtepe. The Ce/Ce* trend reported for Demirtas aligns well with Öznurtepe reporting no Ce depletion indicative of oxic conditions leading up to the oolitic interval marking the extinction (Loope et al., 2013). Hence, as the authors had no geochemical evidence for oxic conditions, their interpretation of consistently oxic redox conditions was based on available palaeontological and sedimentological evidence from Groves et al. (2005). However, at the Global Stratotype Section and Point (GSSP), Meishan, oscillating redox conditions were also identified prior to the extinction, in the fossil-rich Changxing Formation (Li et al., 2016; Shen et al., 2011; Xiang et al., 2020). This emphasises that low degrees of deoxygenation as well as spatially or temporally restricted episodes of anoxia are not necessarily reflected in the fossil and sedimentary record, but might explain the elevated pre-extinction U and Mo enrichments reported here, in the Dolomites (Frank et al., 2025), as well as at Meishan (Xiang et al., 2020).

With the onset of the Permian-Triassic mass extinction both the Cürük Dağ and Öznurtepe sections reveal a shift in RSM EF*, with the Kokarkuyu and Sapadere formations recording generally low EF_{Re}*, EF_U* and EF_{Mo}* (Fig. 5), which are typical for modern marine sediments deposited under oxic conditions (Li et al., 2025). At first glance the Kokarkuyu Formation at Çürük Dağ seems to record higher EF_{Re}* than the underlying Pamucak Formation. However, this is due to most Kokarkuyu Formation samples having Re (and Mo) concentrations under the detection limit, resulting in a biased median value. The presence of an oxygenated environment at Çürük Dağ in the Early Triassic is further supported by an overwhelming presence of negative Ce anomalies (Fig. 2), which is in good agreement with previously presented REY data for Triassic microbialites at Çürük Dağ (Collin et al., 2015). At Öznurtepe, the Sapadere Formation displays negative Ce anomalies for most of the Beslengiler Member as well as the bottom ~5 m of the Taşlıca Member but lacks Ce anomalies in the upper ~ 10 m of the investigated interval. This change in Ce anomalies could be redoxdriven, however, the simultaneous increase in Al combined with the low RSM EF* in this part of the section strongly support that it is likely due to lithological change. At Demirtas, a shift to no Ce anomalies was already recorded for the Beslengiler Member of the Sapadere Formation and interpreted as evidence for the development of an anoxic water column potentially due to a transgression (Loope et al., 2013). The same trend could not be replicated at Öznurtepe (possible due to gaps in the sampling record). However, the lack of negative Ce anomalies can be caused by multiple processes and is not a reliable proxy for anoxia, as demonstrated by the upper part of the Taşlıca Member, which is characterised by oxic RSM EF* signatures, but no negative Ce anomalies. Hence, oxic redox conditions likely prevailed continuously at both localities, suggesting that oxygen availability was not a limiting factor for a potential ecosystem recovery.

5.4. Redox and biodiversity change

The local geochemical redox proxies reported for Çürük Dağ and Öznurtepe reveal complex redox conditions, particularly in the late Permian. Unlike previous studies constraining local redox conditions within the shallow marine Neothethys (Brosse et al., 2019; Heydari et al., 2003; Krystyn et al., 2003; Loope et al., 2013; Richoz et al., 2010), the RSM EF* support the development of local anoxic bottom waters in the Permian pre-extinction interval. However, redox conditions were not consistent but cycled between anoxic and oxic, which is inconsistent with the hypothesis that persistent ultra-shallow marine anoxia was a driver of shallow marine extinctions (Grice et al., 2005; Schobben et al., 2020; Wignall and Twitchett, 1996; Xiang et al., 2020). As an alternative to persistent anoxia, Algeo et al. (2007) proposed that a short-lived introduction of anoxic/euxinic deep water was sufficient to cause the mass extinction at Nhi Thao, Vietnam. While the geochemical data from Çürük Dağ and Öznurtepe do not support upwelling of deoxygenated deep water, both sections support a short-lived development of local anoxia right after the extinction. However, unlike the global extension of deep water anoxia indicated by U isotopes (Brennecka et al., 2011; Lau et al., 2016; Zhang et al., 2020; Zhang et al., 2018a, 2018b), the geochemical signatures typical for anoxia at Cürük Dağ and Öznurtepe do not only coincide with the onset of environmental perturbation indicated by $\delta^{13}C_{carb}$ and onset of the extinction, but also appear significantly prior to the extinction in intervals marked by a rich fossilrecord (Figs. 2, 3, S1, S2) (Angiolini et al., 2007; Aubril and Angiolini, 2009; Crasquin-Soleau et al., 2004; Groves et al., 2005; Verna et al., 2011). This suggests that local bottom water anoxia already developed significantly prior to the Permian-Triassic mass extinction without any visible consequences for marine life. This is potentially due to the RSM EF* reflecting shallow burial conditions or very short-lived anoxic episodes, which might have caused an extirpation of species or physiological stress, but not extinction. The aforementioned begs the question, how could have the observed local anoxic pulse at the beginning of the post-extinction interval caused the extinction if it appears to be a continuation of already dynamic redox conditions rather than a change in local redox conditions?

Alternatively, it is possible that the extinction was triggered by a combination of environmental changes. Increased sea surface temperature, for example, decreases the ocean's metabolic index potentially causing hypoxia for many species (Penn et al., 2018). Temperaturedriven hypoxia has previously been suggested as a likely driver of the Permian-Triassic mass extinction (Foster et al., 2024; Penn et al., 2018), in particular in palaeoequatorial settings similar to the Antalya Nappes. However, meta-analyses on the Permian/Triassic Global Stratotype Section and Point, Meishan, in South China supports that temperaturedriven hypoxia and nutrient stress best explain the Permian-Triassic mass extinction there, irrespective of the development of local redox conditions (Foster et al., 2024). This suggests that changes in sea surface temperature (e.g. Gliwa et al., 2022) and change in primary productivity (e.g., Grasby et al., 2016) rather than local redox were the cause of extinction. Finally, it is important to consider that the observed anoxic episode right above the extinction might also have been a consequence of the extinction, e.g., due to increased oxygen consumption through organic matter degradation by bacteria (Hülse et al., 2021; Schobben et al., 2015) in the absence of filter feeders (e.g., brachiopods, bivalves), rather than a trigger of the extinction itself.

Besides its role as an extinction driver, anoxia has also been suggested as an environmental factor potentially limiting the biotic recovery after the Permian-Triassic extinction (Lau et al., 2016; Twitchett et al., 2004). This is supported by a slow recovery in U isotopes after the extinction, suggesting that seafloor anoxia still affected 5 % of the seafloor compared to 0.2 % before the extinction (Lau et al., 2016). However, this also supports that the majority of the seafloor was likely oxic. The geochemical redox proxies presented here reveal that oxic conditions prevailed at Çürük Dağ and Öznurtepe in the aftermath of the

extinction suggesting sufficient oxygen should have been present to foster a recovery. Thus, based on the currently available data, local anoxia does not appear to play a significant role for biodiversity recovery in the shallow marine Neotethys, suggesting that another environmental factor, such as nutrient stress (Grasby et al., 2016), was limiting the recovery. Besides the persistence of harsh environmental conditions (Foster et al., 2018; Payne et al., 2004), the intensity of the mass extinction event (Hautmann et al., 2015) as well as subsequent biotic crises (Foster et al., 2017; Hofmann et al., 2014; Hofmann et al., 2015b; Payne et al., 2004) have been postulated as causes for the delayed recovery. However, fossil data from Oman (Twitchett et al., 2004), Tibet, Pakistan and Kashmir (Shen et al., 2006) indicate a comparatively rapid recovery of marine organisms in the Neotethys compared to locations in the Palaeotethys (Foster et al., 2018; Hofmann et al., 2015b; Twitchett and Wignall, 1996), although this cannot be generalised (Foster et al., 2019). This emphasises that the environmental and biotic factors governing the recovery of the Permian-Triassic mass extinction likely varied locally, suggesting that post-extinction anoxia as a potential recovery constraint should be assessed on a site-specific basis.

6. Conclusion

Two locations from the Antalya Nappes, Türkiye, representing shallow marine deposition in the western Neotethys across the Permian-Triassic transition, were investigated using local inorganic redox proxies to reconstruct palaeoredox conditions and determine the role of anoxia for biodiversity change. The combination of RSM EF* and REY patterns reveals the potential presence of anoxia around the time of the extinction. The proxies do not support a change from prevailing oxic to anoxic conditions nor a flooding of the shallow shelf by deoxygenated deep water at the onset of the extinction, which have been hypothesised to cause the extinction. Rather episodic anoxic redox condition developed locally and appear to consistently occur during the investigated Permian interval without visible effect on the local fauna up until the extinction, suggesting that they did not create uninhabitable conditions. This raises the question why continued dynamic redox conditions into the onset of the extinction would suddenly cause a biodiversity crisis on its own. After the extinction, the geochemical proxies reveal prevailing oxic conditions confirming that no redox-constraint existed for the immediate recovery period. Thus, the investigated sections suggest that redox alone likely cannot explain the biodiversity change within the shallow marine western Neotethys across the Permian-Triassic transition.

Supplementary data to this article can be found online at https://doi.org/10.1016/j.chemgeo.2025.123108.

CRediT authorship contribution statement

Anja B. Frank: Writing – original draft, Visualization, Methodology, Investigation, Formal analysis, Conceptualization. Baran Karapunar: Writing – review & editing, Investigation. Stephen E. Grasby: Writing – review & editing, Methodology, Investigation. Erdal Koşun: Writing – review & editing, Investigation. Niko Lahajnar: Writing – review & editing, Methodology. Mónica Alejandra Gómez Correa: Writing – review & editing, Investigation. Stella Z. Buchwald: Writing – review & editing, Investigation. Marc Metzke: Writing – review & editing, Methodology. William J. Foster: Writing – review & editing, Visualization, Investigation, Funding acquisition, Conceptualization.

Declaration of competing interest

The authors declare that they have no known competing financial interests or personal relationships that could have appeared to influence the work reported in this paper.

Acknowledgements

The authors would like to acknowledge the funding provided by the DFG grant FO1297/1. We thank Saliha Dündar and Jörn Peckmann for assisting us with fieldwork. Finally, we extend our thanks to the handling editor, Dr. Vasileios Mavromatis, as well as Dr. Pulkit Singh and another anonymous reviewer for their constructive input, which helped improve our work.

Data availabilityThe complete data set compiled for this study is included in the supplement (Table S2) and publicly available under the following link: https://zenodo.org/records/17348303

The complete data set compiled for this study is included in the supplement (Table S2) and publicly available under the following link: https://zenodo.org/records/17348303

References

- Algeo, T.J., Li, C., 2020. Redox classification and calibration of redox thresholds in sedimentary systems. Geochim. Cosmochim. Acta 287, 8–26. https://doi.org/ 10.1016/j.gca.2020.01.055.
- Algeo, T.J., Ellwood, B., Nguyen, T.K.T., Rowe, H., Maynard, J.B., 2007. The Permian–Triassic boundary at Nhi Tao, Vietnam: evidence for recurrent influx of sulfidic watermasses to a shallow-marine carbonate platform. Palaeogeogr. Palaeoclimatol. Palaeoecol. 252, 304–327. https://doi.org/10.1016/j. palaeo.2006.11.055.
- Algeo, T.J., Hinnov, L., Moser, J., Maynard, J.B., Elswick, E., Kuwahara, K., Sano, H., 2010. Changes in productivity and redox conditions in the Panthalassic Ocean during the latest Permian. Geology 38, 187–190. https://doi.org/10.1130/ G30483 1
- Allen, B.J., Clapham, M.E., Saupe, E.E., Wignall, P.B., Hill, D.J., Dunhill, A.M., 2023. Estimating spatial variation in origination and extinction in deep time: a case study using the Permian–Triassic marine invertebrate fossil record. Paleobiology 49, 509–526. https://doi.org/10.1017/pab.2023.1.
- Altiner, D., Zaninetti, L., 1981. Le Trias dans la région de Pinarbasi, Taurus oriental, Turquie: unités lithologiques, micropaléonto-logie, milieux de dépôt. Riv. Ital. Paleont. 86, 705–760.
- Angiolini, L., Carabelli, L., Nicora, A., Crasquin-Soleau, S., Marcoux, J., Rettori, R., 2007. Brachiopods and other fossils from the Permo-Triassic boundary beds of the Antalya Nappes (SW Taurus, Turkey). Geobios 40, 715–729. https://doi.org/10.1016/j. geobios.2007.01.007.
- Aubril, R.L., Angiolini, L., 2009. Permian Trilobites from Antalya Province, Turkey, and Enrollment in late Palaeozoic Trilobites. Turk. J. Earth Sci. https://doi.org/10.3906/ yer-0801-5.
- Baud, A., Richoz, S., Marcoux, J., 2005. Calcimicrobial cap rocks from the basal Triassic units: western Taurus occurrences (SW Turkey). Comp. Rend. Palevol. 4, 569–582. https://doi.org/10.1016/j.crpv.2005.03.001.
- Blakey, R., 2012. Global Paleogeography (Acessed at http://www2.nau.edu/rcb7/globaltext2.html on 30 July 2012).
- Brennecka, G.A., Herrmann, A.D., Algeo, T.J., Anbar, A.D., 2011. Rapid expansion of oceanic anoxia immediately before the end-Permian mass extinction. Proc. Natl. Acad. Sci. 108, 17631–17634. https://doi.org/10.1073/pnas.1106039108.
- Brosse, M., Bucher, H., Baud, A., Frisk, Å.M., Goudemand, N., Hagdorn, H., Nützel, A., Ware, D., Hautmann, M., 2019. New data from Oman indicate benthic high biomass productivity coupled with low taxonomic diversity in the aftermath of the Permian–Triassic Boundary mass extinction. Lethaia 52, 165–187. https://doi.org/10.1111/jet.12281.
- Buchwald, S.Z., Frank, A.B., Birgel, D., Senger, K., Mosociova, T., Pei, Y., Beaty, B., Tarhan, L., Galasso, F., GomezCorrea, M.A., Grasby, S.E., Struck, U., Steinkrauss, R., Gliwa, J., Lahajnar, N., Peckmann, J., Foster, W.J., 2025. Reconstructing environmental and microbial ecosystem changes across the Permian-Triassic mass extinction at Lusitaniadalen, Svalbard. ESS Open Archiv. https://doi.org/10.22541/essoar.175766816.64475408/v1.
- Burgess, S.D., Bowring, S.A., 2015. High-precision geochronology confirms voluminous magmatism before, during, and after Earth's most severe extinction. Sci. Adv. 1, e1500470. https://doi.org/10.1126/sciadv.1500470.
- Burgess, S.D., Muirhead, J.D., Bowring, S.A., 2017. Initial pulse of Siberian Traps sills as the trigger of the end-Permian mass extinction. Nat. Commun. 8, 164. https://doi. org/10.1038/s41467-017-00083-9.
- Cao, C., Love, G.D., Hays, L.E., Wang, W., Shen, S., Summons, R.E., 2009. Biogeochemical evidence for euxinic oceans and ecological disturbance presaging the end-Permian mass extinction event. Earth Planet. Sci. Lett. 281, 188–201. https://doi.org/10.1016/j.epsl.2009.02.012.
- Chen, Z.-Q., Yang, H., Luo, M., Benton, M.J., Kaiho, K., Zhao, L., Huang, Y., Zhang, K., Fang, Y., Jiang, H., Qiu, H., Li, Y., Tu, C., Shi, L., Zhang, L., Feng, X., Chen, L., 2015. Complete biotic and sedimentary records of the Permian–Triassic transition from Meishan section, South China: ecologically assessing mass extinction and its aftermath. Earth Sci. Rev. 149, 67–107. https://doi.org/10.1016/j.earscirev.2014.10.005.

A.B. Frank et al. Chemical Geology 696 (2025) 123108

- Collin, P.Y., Kershaw, S., Tribovillard, N., Forel, M.B., Crasquin, S., 2015. Geochemistry of post-extinction microbialites as a powerful tool to assess the oxygenation of shallow marine water in the immediate aftermath of the end-Permian mass extinction. Int. J. Earth Sci. (Geol. Rundsch.) 104, 1025–1037. https://doi.org/10.1007/s00531-014-1125-3.
- Crasquin-Soleau, S., Richoz, S., Marcoux, J., Angiolini, L., Nicora, A., Baud, A., 2002. Les événements de la limite Permien–Trias: derniers survivants et/ou premiers recolonisateurs parmi les ostracodes du Taurus (Sud-Ouest de la Turquie). C. R. Geosci. 334, 489–495. https://doi.org/10.1016/S1631-0713(02)01782-0.
- Crasquin-Soleau, S., Marcoux, J., Angiolini, L., Richoz, S., Nicora, A., Baud, A., Bertho, Y., 2004. A new ostracode fauna from the Permian-Triassic boundary in Turkey (Taurus, Antalya Nappes). Micropaleontology 50, 281–295. https://doi.org/ 10.2113/50.3.281.
- Demirtaş, F., 2018. Antalya civarındaki Permiyen-triyas geçişinin Sedimantolojik, Petrografik Ve Jeokimyasal açıdan Incelenmesi / Investigation of Permian-triassic Boundary around Antalya in Terms of Sedimentology, Petrography and Geochemistry (PhD Thesis). Akdeniz Üniversitesi, Antalya, Turkey.
- Elderfield, H., Greaves, M.J., 1982. The rare earth elements in seawater. Nature 296, 214.
- Foster, W.J., Twitchett, R.J., 2014. Functional diversity of marine ecosystems after the late Permian mass extinction event. Nat. Geosci. 7, 233–238. https://doi.org/ 10.1038/ngeo2079.
- Foster, W.J., Danise, S., Price, G.D., Twitchett, R.J., 2017. Subsequent biotic crises delayed marine recovery following the late Permian mass extinction event in northern Italy. PloS One 12, e0172321. https://doi.org/10.1371/journal. pone.0172321.
- Foster, W.J., Lehrmann, D.J., Yu, M., Ji, L., Martindale, R.C., 2018. Persistent Environmental stress delayed the recovery of marine communities in the aftermath of the latest Permian mass extinction. Paleoceanogr. Paleoclimatol. 33, 338–353. https://doi.org/10.1002/2018PA003328.
- Foster, W.J., Lehrmann, D.J., Hirtz, J.A., White, M., Yu, M., Li, J., Martindale, R.C., 2019. Early Triassic benthic invertebrates from the Great Bank of Guizhou, South China: systematic palaeontology and palaeobiology. Pap. Palaeontol. 5, 613–656. https://doi.org/10.1002/spp2.1252.
- Foster, W.J., Asatryan, G., Rauzi, S., Botting, J.P., Buchwald, S.Z., Lazarus, D.B., Isson, T., Renaudie, J., Kiessling, W., 2023. Response of siliceous marine organisms to the Permian-Triassic climate crisis based on new findings from Central Spitsbergen, Svalbard. Paleoceanogr. Paleoclimatol. 38, e2023PA004766. https://doi.org/ 10.1029/2023PA004766
- Foster, W.J., Frank, A.B., Li, Q., Danise, S., Wang, X., Peckmann, J., 2024. Thermal and nutrient stress drove Permian-Triassic shallow marine extinctions. In: Cambridge Prisms: Extinction, pp. 1–25. https://doi.org/10.1017/ext.2024.9.
- Frank, A.B., Klaebe, R.M., Xu, L., Frei, R., 2021. Constraining shallow seawater oxygenation for the Yangtze Platform during the early Cambrian. Paleoceanogr. Paleoclimatol. 36, e2021PA004282. EarthArXiv. https://doi.org/10.1029/2021 PA004282.
- Frank, A.B., Warncke-Rüting, E., Grasby, S., Kustatscher, E., Prinoth, H., Poulton, S.W., Xiong, Y., Korn, D., Gliwa, J., Foster, W., 2025. Oxic Conditions in Shallow Marine Settings During the Permian-Triassic Mass Extinction. https://doi.org/10.31223/ VELIUSE
- Gliwa, J., Ghaderi, A., Leda, L., Schobben, M., Tomás, S., Foster, W.J., Forel, M.-B., Ghanizadeh Tabrizi, N., Grasby, S.E., Struck, U., Ashouri, A.R., Korn, D., 2020. Aras Valley (northwest Iran): high-resolution stratigraphy of a continuous central Tethyan Permian–Triassic boundary section. Fossil Rec. 23, 33–69. https://doi.org/10.5194/fr.23-33-2020
- Gliwa, J., Wiedenbeck, M., Schobben, M., Ullmann, C.V., Kiessling, W., Ghaderi, A., Struck, U., Korn, D., 2022. Gradual warming prior to the end-Permian mass extinction. Palaeontology 65, e12621. https://doi.org/10.1111/pala.12621.
- Grasby, S.E., Beauchamp, B., 2008. Intrabasin variability of the carbon-isotope record across the Permian-Triassic transition, Sverdrup Basin, Arctic Canada. Chem. Geol. 253, 141–150. https://doi.org/10.1016/j.chemgeo.2008.05.005.
- Grasby, S.E., Sanei, H., Beauchamp, B., 2011. Catastrophic dispersion of coal fly ash into oceans during the latest Permian extinction. Nat. Geosci. 4, 104–107. https://doi. org/10.1038/ngeo1069.
- Grasby, S.E., Beauchamp, B., Bond, D.P.G., Wignall, P., Talavera, C., Galloway, J.M., Piepjohn, K., Reinhardt, L., Blomeier, D., 2015. Progressive environmental deterioration in northwestern Pangea leading to the latest Permian extinction. GSA Bull. 127, 1331–1347. https://doi.org/10.1130/B31197.1.
- Grasby, S.E., Beauchamp, B., Knies, J., 2016. Early Triassic productivity crises delayed recovery from world's worst mass extinction. Geology 44, 779–782. https://doi.org/ 10.1130/G38141.1.
- Grice, K., Cao, C., Love, G.D., Böttcher, M.E., Twitchett, R.J., Grosjean, E., Summons, R. E., Turgeon, S.C., Dunning, W., Jin, Y., 2005. Photic zone Euxinia during the Permian-Triassic superanoxic event. Science. https://doi.org/10.1126/science.1104323.
- Groves, J.R., Altiner, D., Rettori, R., 2005. Extinction, Survival, and Recovery of Lagenide Foraminifers in the Permian–Triassic Boundary Interval, Central Taurides, Turkey, 79, pp. 1–38. https://doi.org/10.1666/0022-3360(2005)79%255B1: ESAROL%255D2.0.CO;2.
- Hautmann, M., Bagherpour, B., Brosse, M., Frisk, Å., Hofmann, R., Baud, A., Nützel, A., Goudemand, N., Bucher, H., 2015. Competition in slow motion: the unusual case of benthic marine communities in the wake of the end-Permian mass extinction. Palaeontology 58, 871–901. https://doi.org/10.1111/pala.12186.
- Hays, L.E., Beatty, T., Henderson, C.M., Love, G.D., Summons, R.E., 2007. Evidence for photic zone euxinia through the end-Permian mass extinction in the Panthalassic Ocean (Peace River Basin, Western Canada). In: Palaeoworld, Contributions to

Permian and Carboniferous Stratigraphy, Brachiopod Palaeontology and End-Permian Mass Extinctions, In Memory of Professor Yu-Gan Jin, 16, pp. 39–50. https://doi.org/10.1016/j.palwor.2007.05.008.

- Heydari, E., Hassanzadeh, J., Wade, W.J., Ghazi, A.M., 2003. Permian–Triassic boundary interval in the Abadeh section of Iran with implications for mass extinction: Part 1 sedimentology. Palaeogeogr. Palaeoclimatol. Palaeoecol. 193, 405–423. https://doi.org/10.1016/S0031-0182(03)00258-X.
- Hofmann, R., Hautmann, M., Brayard, A., Nützel, A., Bylund, K.G., Jenks, J.F., Vennin, E., Olivier, N., Bucher, H., 2014. Recovery of benthic marine communities from the end-Permian mass extinction at the low latitudes of eastern Panthalassa. Palaeontology 57, 547–589. https://doi.org/10.1111/pala.12076.
- Hofmann, R., Buatois, L.A., MacNaughton, R.B., Mángano, M.G., 2015a. Loss of the sedimentary mixed layer as a result of the end-Permian extinction. Palaeogeogr. Palaeoclimatol. Palaeoecol. 428, 1–11. https://doi.org/10.1016/j. palaeo. 2015.03.036
- Hofmann, Richard, Hautmann, M., Bucher, H., 2015b. Recovery dynamics of benthic marine communities from the lower Triassic Werfen Formation, northern Italy. Lethaia 48, 474–496. https://doi.org/10.1111/let.12121.
- Hülse, D., Lau, K.V., van de Velde, S.J., Arndt, S., Meyer, K.M., Ridgwell, A., 2021. End-Permian marine extinction due to temperature-driven nutrient recycling and euxinia. Nat. Geosci. 14, 862–867. https://doi.org/10.1038/s41561-021-00829-7.
- Isozaki, Y., 1997. Permo-Triassic Boundary Superanoxia and Stratified Superocean: Records from lost Deep Sea. Science 276, 235–238. https://doi.org/10.1126/science.276.5310.235.
- Joachimski, M.M., Lai, X., Shen, S., Jiang, H., Luo, G., Chen, B., Chen, J., Sun, Y., 2012. Climate warming in the latest Permian and the Permian–Triassic mass extinction. Geology 40, 195–198. https://doi.org/10.1130/G32707.1.
- Karapunar, B., Wang, X., Frank, A.B., Gürsoy, M., Buchwald, S.Z., Gómez Correa, M.A., Liu, Z., Xu, X., Meng, L., Demir, D., Koşun, E., Foster, W.J., 2025. Environmental and ecological changes across the Permian–Triassic transition in Türkiye: integrating virtual outcrop models and new fieldwork data. EarthArXiv. https://doi.org/ 10.31223/X5KO9B.
- Kershaw, S., Crasquin, S., Forel, M.-B., Randon, C., Collin, P.-Y., Kosun, E., Richoz, S., Baud, A., 2011. Earliest Triassic microbialites in Çürük Dag, southern Turkey: composition, sequences and controls on formation. Sedimentology 58, 739–755. https://doi.org/10.1111/j.1365-3091.2010.01181.x.
- Kershaw, S., Crasquin, S., Li, Y., Collin, P.-Y., Forel, M.-B., Mu, X., Baud, A., Wang, Y., Xie, S., Maurer, F., Guo, L., 2012. Microbialities and global environmental change across the Permian–Triassic boundary: a synthesis. Geobiology 10, 25–47. https://doi.org/10.1111/j.1472-4669.2011.00302.x.
- Knies, J., Grasby, S.E., Beauchamp, B., Schubert, C.J., 2013. Water mass denitrification during the latest Permian extinction in the Sverdrup Basin, Arctic Canada. Geology 41, 167–170. https://doi.org/10.1130/G33816.1.
- Knoll, A.H., Bambach, R.K., Canfield, D.E., Grotzinger, J.P., 1996. Comparative Earth history and late Permian Mass Extinction. Science 273, 452–457. https://doi.org/ 10.1126/science.273.5274.452.
- Korte, C., Kozur, H.W., 2010. Carbon-isotope stratigraphy across the Permian–Triassic boundary: a review. J. Asian Earth Sci. 39, 215–235. https://doi.org/10.1016/j. iseaes.2010.01.005.
- Krewer, C., Poulton, S.W., Newton, R.J., März, C., Mills, B.J.W., Wagner, T., 2024. Controls on the termination of Cretaceous Oceanic Anoxic Event 2 in the Tarfaya Basin, Morocco. Am. J. Sci. 324. https://doi.org/10.2475/001c.118797.
- Krystyn, L., Richoz, S., Baud, A., Twitchett, R.J., 2003. A unique Permian–Triassic boundary section from the Neotethyan Hawasina Basin, Central Oman Mountains. In: Palaeogeography, Palaeoclimatology, Palaeoecology, Pangea special issue selected papers from the Pangea Symposium, Muscat, January 2001, 191, pp. 329–344. https://doi.org/10.1016/S0031-0182(02)00670-3.
- Kump, L.R., Pavlov, A., Arthur, M.A., 2005. Massive release of hydrogen sulfide to the surface ocean and atmosphere during intervals of oceanic anoxia. Geology 33, 397–400. https://doi.org/10.1130/G21295.1.
- Lau, K.V., Maher, K., Altiner, D., Kelley, B.M., Kump, L.R., Lehrmann, D.J., Silva-Tamayo, J.C., Weaver, K.L., Yu, M., Payne, J.L., 2016. Marine anoxia and delayed Earth system recovery after the end-Permian extinction. Proc. Natl. Acad. Sci. 113, 2360–2365. https://doi.org/10.1073/pnas.1515080113.
- Lawrence, M.G., Greig, A., Collerson, K.D., Kamber, B.S., 2006. Rare Earth Element and Yttrium Variability in South East Queensland Waterways. Aquat. Geochem. 12, 39–72. https://doi.org/10.1007/s10498-005-4471-8.
- Li, W., Li, X., Li, Z., 2005. Neoproterozoic bimodal magmatism in the Cathaysia Block of South China and its tectonic significance. Precambrian Res. 136, 51–66. https://doi. org/10.1016/j.precamres.2004.09.008.
- Li, G., Wang, Y., Shi, G.R., Liao, W., Yu, L., 2016. Fluctuations of redox conditions across the Permian–Triassic boundary—new evidence from the GSSP section in Meishan of South China. Palaeogeogr. Palaeoclimatol. Palaeoecol. 448, 48–58. https://doi.org/ 10.1016/j.palaeo.2015.09.050.
- Li, S., Wignall, P.B., Poulton, S.W., 2025. Co-application of rhenium, vanadium, uranium and molybdenum as paleo-redox proxies: Insight from modern and ancient environments. Chem. Geol. 674, 122565. https://doi.org/10.1016/j. chemgeo.2024.122565.
- Loope, G.R., Kump, L.R., Arthur, M.A., 2013. Shallow water redox conditions from the Permian–Triassic boundary microbialite: the rare earth element and iodine geochemistry of carbonates from Turkey and South China. Chem. Geol. 351, 195–208. https://doi.org/10.1016/j.chemgeo.2013.05.014.
- Lys, M., Marcoux, J., 1978. Les niveaux du Permien supérieurdes Nappes d'Antalya (Taurides occidentales, Turquie). C. R. Acad. Sci. 286, 1417–1420.
- Martindale, R.C., Foster, W.J., Velledits, F., 2019. The survival, recovery, and diversification of metazoan reef ecosystems following the end-Permian mass

- extinction event. Palaeogeogr. Palaeoclimatol. Palaeoecol. 513, 100–115. https://doi.org/10.1016/j.palaeo.2017.08.014.
- Morse, J.W., Mackenzie, F.T., 1990. Geochemistry of Sedimentary Carbonates. Elsevier.
- Muscente, A.D., Prabhu, A., Zhong, H., Eleish, A., Meyer, M.B., Fox, P., Hazen, R.M., Knoll, A.H., 2018. Quantifying ecological impacts of mass extinctions with network analysis of fossil communities. Proc. Natl. Acad. Sci. 115, 5217–5222. https://doi.org/10.1073/pnas.1719976115.
- Nabbefeld, B., Grice, K., Twitchett, R.J., Summons, R.E., Hays, L., Böttcher, M.E., Asif, M., 2010. An integrated biomarker, isotopic and palaeoenvironmental study through the late Permian event at Lusitaniadalen, Spitsbergen. Earth Planet. Sci. Lett. 291, 84–96. https://doi.org/10.1016/j.epsl.2009.12.053.
- Nothdurft, L.D., Webb, G.E., Kamber, B.S., 2004. Rare earth element geochemistry of late Devonian reefal carbonates, Canning Basin, Western Australia: confirmation of a seawater REE proxy in ancient limestones. Geochim. Cosmochim. Acta 68, 263–283. https://doi.org/10.1016/S0016-7037(03)00422-8.
- Özgül, N., 1985. Alanya tectonic window and geology of its western part. In: Presented at the Ketin Symposium, pp. 97–120.
- Payne, J.L., Lehrmann, D.J., Wei, J., Orchard, M.J., Schrag, D.P., Knoll, A.H., 2004. Large Perturbations of the Carbon Cycle during Recovery from the End-Permian Extinction. Science 305, 506–509. https://doi.org/10.1126/science.1097023.
- Penn, J.L., Deutsch, C., Payne, J.L., Sperling, E.A., 2018. Temperature-dependent hypoxia explains biogeography and severity of end-Permian marine mass extinction. Science 362, eaat1327. https://doi.org/10.1126/science.aat1327.
- Proemse, B.C., Grasby, S.E., Wieser, M.E., Mayer, B., Beauchamp, B., 2013. Molybdenum isotopic evidence for oxic marine conditions during the latest Permian extinction. Geology 41, 967–970. https://doi.org/10.1130/G34466.1.
- Richoz, S., 2006. Stratigraphie et variations isotopiques du carbone dans le Permien supérieur et le Trias inférieur de quelques localités de la Néotéthys (Turquie, Oman et Iran) (PhD Thesis). Université de Lausanne, Lausanne.
- Richoz, S., Krystyn, L., Baud, A., Brandner, R., Horacek, M., Mohtat-Aghai, P., 2010. Permian–Triassic boundary interval in the Middle East (Iran and N. Oman): progressive environmental change from detailed carbonate carbon isotope marine curve and sedimentary evolution. J. Asian Earth Sci. 39, 236–253. https://doi.org/ 10.1016/i.jseaes.2009.12.014.
- Rodler, A.S., Frei, R., Gaucher, C., Korte, C., Rosing, S.A., Germs, G.J.B., 2017.
 Multiproxy isotope constraints on ocean compositional changes across the late
 Neoproterozoic Ghaub glaciation, Otavi Group, Namibia. Precambr. Res. 298, 306–324. https://doi.org/10.1016/j.precamres.2017.05.006.
- Şahin, N., Altiner, D., 2019. Testing of Permian–lower Triassic stratigraphic data in a half-graben/tilt-block system: evidence for the initial rifting phase in Antalya Nappes. Can. J. Earth Sci. 56, 1262–1283. https://doi.org/10.1139/cjes-2018-0169.
- Schobben, M., Stebbins, A., Ghaderi, A., Strauss, H., Korn, D., Korte, C., 2015.
 Flourishing Ocean drives the end-Permian marine mass extinction. Proc. Natl. Acad.
 Sci. 112, 10298–10303. https://doi.org/10.1073/pnas.1503755112.
- Schobben, M., Foster, W.J., Sleveland, A.R.N., Zuchuat, V., Svensen, H.H., Planke, S., Bond, D.P.G., Marcelis, F., Newton, R.J., Wignall, P.B., Poulton, S.W., 2020. A nutrient control on marine anoxia during the end-Permian mass extinction. Nat. Geosci. 13, 640–646. https://doi.org/10.1038/s41561-020-0622-1.
- Scotese, C.R., Langford, R.P., 1995. Pangea and the Paleogeography of the Permian. In: Scholle, P.A., Peryt, T.M., Ulmer-Scholle, D.S. (Eds.), The Permian of Northern Pangea, Paleogeography, Paleoclimates, vol. 1. Stratigraphy. Springer, Berlin, Heidelberg, pp. 3–19. https://doi.org/10.1007/978-3-642-78593-1_1.
- Shen, S.Z., Cao, C.-Q., Henderson, C.M., Wang, X.-D., Shi, G.R., Wang, Y., Wang, W., 2006. End-Permian mass extinction pattern in the northern peri-Gondwanan region. Palaeoworld 15, 3–30. https://doi.org/10.1016/j.palwor.2006.03.005.
- Shen, W., Lin, Y., Xu, L., Li, J., Wu, Y., Sun, Y., 2007. Pyrite framboids in the Permian–Triassic boundary section at Meishan, China: evidence for dysoxic deposition. Palaeogeogr. Palaeoclimatol. Palaeoecol. 253, 323–331. https://doi.org/ 10.1016/j.palaeo.2007.06.005.
- Shen, Y., Farquhar, J., Zhang, H., Masterson, A., Zhang, T., Wing, B.A., 2011. Multiple S-isotopic evidence for episodic shoaling of anoxic water during late Permian mass extinction. Nat. Commun. 2, 210. https://doi.org/10.1038/ncomms1217.
- Song, Haijun, Wignall, P.B., Tong, J., Bond, D.P.G., Song, Huyue, Lai, X., Zhang, K., Wang, H., Chen, Y., 2012. Geochemical evidence from bio-apatite for multiple oceanic anoxic events during Permian–Triassic transition and the link with end-Permian extinction and recovery. Earth Planet. Sci. Lett. 353–354, 12–21. https://doi.org/10.1016/j.epsl.2012.07.005.

- Stampfli, G., Marcoux, J., Baud, A., 1991. Tethyan margins in space and time. Palaeogeogr. Palaeoclimatol. Palaeoecol. 87, 373–409. https://doi.org/10.1016/0031-0182(91)90142-E.
- Svensen, H.H., Jones, M.T., Mather, T.A., 2023. Large Igneous Provinces and the Release of Thermogenic Volatiles from Sedimentary Basins. Elements 19, 282–288. https:// doi.org/10.2138/gselements.19.5.282.
- Taylor, S.R., McLennan, S.M., 1985. The Continental Crust: Its Composition and Evolution, OSTI ID: 6582885 (United States).
- Tostevin, R., Shields, G.A., Tarbuck, G.M., He, T., Clarkson, M.O., Wood, R.A., 2016. Effective use of cerium anomalies as a redox proxy in carbonate-dominated marine settings. Chem. Geol. 438, 146–162. https://doi.org/10.1016/j.
- Tribovillard, N., Algeo, T.J., Lyons, T., Riboulleau, A., 2006. Trace metals as paleoredox and paleoproductivity proxies: An update. Chem. Geol. 232, 12–32. https://doi.org/ 10.1016/j.chemgeo.2006.02.012.
- Tribovillard, N., Algeo, T.J., Baudin, F., Riboulleau, A., 2012. Analysis of marine environmental conditions based on molybdenum-uranium covariation—applications to Mesozoic paleoceanography. Chem. Geol. 324–325, 46–58. https://doi.org/10.1016/j.chemgeo.2011.09.009.
- Twitchett, R.J., Wignall, P.B., 1996. Trace fossils and the aftermath of the Permo-Triassic mass extinction: evidence from northern Italy. Palaeogeogr. Palaeoclimatol. Palaeoecol. 124, 137–151. https://doi.org/10.1016/0031-0182(96)00008-9.
- Twitchett, R.J., Krystyn, L., Baud, A., Wheeley, J.R., Richoz, S., 2004. Rapid marine recovery after the end-Permian mass-extinction event in the absence of marine anoxia. Geology 32, 805–808. https://doi.org/10.1130/G20585.1.
- Verna, V., Angiolini, L., Baud, A., Crasquin, S., Nicora, A., 2011. Guadalupian brachiopods from western Taurus, Turkey. Riv. Ital. Paleontol. Stratigr. 117. https:// doi.org/10.13130/2039-4942/5963.
- Wallace, M.W., Hood, A., Shuster, A., Greig, A., Planavsky, N.J., Reed, C.P., 2017.
 Oxygenation history of the Neoproterozoic to early Phanerozoic and the rise of land plants. Earth Planet. Sci. Lett. 466, 12–19. https://doi.org/10.1016/j.epsl.2017.02.046.
- Wignall, P.B., Hallam, A., 1992. Anoxia as a cause of the Permian/Triassic mass extinction: facies evidence from northern Italy and the western United States. Palaeogeogr. Palaeoclimatol. Palaeoecol. 93, 21–46. https://doi.org/10.1016/0031-0182(92)90182-5.
- Wignall, P.B., Twitchett, R.J., 1996. Oceanic Anoxia and the End Permian Mass Extinction. Science 272, 1155–1158. https://doi.org/10.1126/ science 272, 5265, 1155
- Xiang, L., Zhang, H., Schoepfer, S.D., Cao, C., Zheng, Q., Yuan, D., Cai, Y., Shen, S., 2020. Oceanic redox evolution around the end-Permian mass extinction at Meishan, South China. Palaeogeogr. Palaeoclimatol. Palaeoecol. 544, 109626. https://doi.org/ 10.1016/j.palaeo.2020.109626.
- Yang, F., Li, S., An, K.Y., Bond, D.P.G., Ao, R., Wu, X.B., Ma, L.L., Sun, Y.D., 2024. Re-evaluating water column reoxygenation during the end Permian mass extinction. Geochem. Geophys. Geosyst. 25, e2024GC011779. https://doi.org/10.1029/2024GC011779.
- Zhang, F., Algeo, T.J., Romaniello, S.J., Cui, Y., Zhao, L., Chen, Z.-Q., Anbar, A.D., 2018a. Congruent Permian-Triassic 8238U records at Panthalassic and Tethyan sites: Confirmation of global-oceanic anoxia and validation of the U-isotope paleoredox proxy. Geology 46, 327–330. https://doi.org/10.1130/G39695.1.
- Zhang, F., Romaniello, S.J., Algeo, T.J., Lau, K.V., Clapham, M.E., Richoz, S., Herrmann, A.D., Smith, H., Horacek, M., Anbar, A.D., 2018b. Multiple episodes of extensive marine anoxia linked to global warming and continental weathering following the latest Permian mass extinction. Sci. Adv. 4, e1602921. https://doi.org/ 10.1126/sciadv.1602921.
- Zhang, F., Shen, S., Cui, Y., Lenton, T.M., Dahl, T.W., Zhang, H., Zheng, Q., Wang, W., Krainer, K., Anbar, A.D., 2020. Two distinct episodes of marine anoxia during the Permian-Triassic crisis evidenced by uranium isotopes in marine dolostones. Geochim. Cosmochim. Acta 287, 165–179. https://doi.org/10.1016/j.gca.2020.01.032.
- Zhang, H., Zhang, F., Chen, J., Erwin, D.H., Syverson, D.D., Ni, P., Rampino, M., Chi, Z., Cai, Y., Xiang, L., Li, W., Liu, S.-A., Wang, R., Wang, X., Feng, Z., Li, H., Zhang, T., Cai, H., Zheng, W., Cui, Y., Zhu, X., Hou, Z., Wu, F., Xu, Y., Planavsky, N., Shen, S., 2021. Felsic volcanism as a factor driving the end-Permian mass extinction. Sci. Adv. 7, eabh1390. https://doi.org/10.1126/sciadv.abh1390.